Corresponding Author: Dr. Yingfang Zhou, Ph.D

Corresponding Author's Institution: University of Aberceen

First Author: Hao Wu

Order of Authors: Hao Wu; Yingfang Zhou, Ph.D; Yanbin Yao; Kejian Wu

Abstract: To better understand the fractal characteristics of coal fracture network and find the relation between 2D and 3D fractal dimensions, we utilized the improved box counting method to calculate 2D and 3D fractal dimensions based on high resolution CT images of 4 coal samples (Ro from 2.915% to 4.69%). Based on the calculated 2D and 3D fractal dimension and porosity, the size of representative element volume (REV), the relationship between D_{f2} and D_{f3} and the relationship between porosity and fractal dimension are investigated extensively.
It is noticed that the fractal dimension-based REV of coal is smaller than the porosity-based REV. As the complement of previous theoretical studies, it is proved that porosity has an exponential relationship with fractal dimension. By deducing formulas based on fractal theory, a new way to get the lower self-similar region size from relation between porosity and fractal dimension is provided. Evidently, the relation between 2D and 3D fractal dimension of coal could be expressed as $D_{f3}=CD_{f2}+ \varphi$, and the slope of the line, C, depends on the average 2D fractal dimension of the sample. Finally, the reference of the relation between D_{f2} and C of high rank coal is provided as $C= -0.75D_{f2} +2.75$.

Research Data Related to this Submission

There are no linked research data sets for this submission. The following reason is given:
Data will be made available on request

1 # Imaged based fractal characterization of micro-fracture structure in

2 # coal

3 **Hao Wu[a,b,c], Yingfang Zhou[c*], Yanbin Yao[ad*], Kejian Wu[c]**

4 [a] School of Energy resource, China University of Geosciences, Beijing 100083, China
5 [b] Beijing Key Laboratory of Unconventional Natural Gas Geology Evaluation and Development Engineering, China
6 University of Geosciences, Beijing 100083, China
7 [c] School of Engineering, University of Aberdeen, Aberdeen, AB243UE, United Kingdom
8 [d] Coal Reservoir Laboratory of National Engineering Research Center of CBM Development & Utilization, China
9 University of Geosciences, Beijing 100083, China

10 ## Abstract

11   To better understand the fractal characteristics of coal fracture network and find the relation

12 between 2D and 3D fractal dimensions, the improved box counting method was utilized to calculate

13 2D and 3D fractal dimensions based on high resolution CT images of 4 coal samples (R_o from 2.915%

14 to 4.69%). Based on the calculated 2D and 3D fractal dimension, the size of representative element

15 volume (REV), the relationship between D_{f2} and D_{f3} and the relationship between porosity and

16 fractal dimension were investigated extensively. As the complement of previous theoretical studies,

17 the exponential relationship between porosity and fractal dimension was proved. By deducing

18 formulas based on fractal theory, a novel way to get the lower self-similar region size from the

19 relation between porosity and fractal dimension was provided. Evidently, the relation between 2D

20 and 3D fractal dimension of coal could be expressed as $D_{f3} = CD_{f2} + 1$, and the slope of the line, C,

21 depends on the average 2D fractal dimension of the sample.

22 ## Key words

23 Fractal dimension; Coal; Micro-CT images; Box-counting method, REV

1. Introduction

The fractal theory was proposed initially by Mandelbrot [1] to explore the complexity of the natural world, and it was widely applied to characterize complexed pore structure. Avnir, *et al*. [2] reported that the surface of most materials, at molecular scale, are fractal; with the application of Scanning Electron Microscopy (SEM), Katz and Thompson [3] illustrated that the pore structure of sandstones is typical self-similar and thus could be characterized by fractal theory. Since then, fractal characterization of porous media have been studied extensively over the past three decades [4-9].

According to the fractal theory proposed by Mandelbrot, the pores size distribution of a self-similar pore structure satisfies the cumulative distribution function as given in Eq. (1),

$$N(L) \propto L^{-D} \qquad (1)$$

here $N(L)$ is cumulative pore with size larger than L, and D is the fractal dimension. In the porous media research community, the fractal dimension is normally determined by experimental measurements, such as mercury intrusion curve [10], Small-angle Neutron Scattering measurement [11,12] and Nuclear Magnetic Resonance measurements [13]. Besides these indirect measurements, fractal dimension of pore space and size normally estimated with the well-known box-counting method from two-dimension rock images [14,15]. However, fractal dimensions measured through different experiments are different. For example, fractal dimensions estimated from N_2 adsorption experiment represent the fractal dimension of surface and volumetric roughness, the fractal dimension measured through mercury intrusion is volumetric fractal dimension, while fractal dimension inferred from NMR data represents pore size distribution fractal. The fractal dimension calculated by box counting method represent the fractal dimension of pore volume/area size and distribution in space, therefore, the fractal dimension calculated through box counting method is a valuable parameter to study seepage properties of porous media [16-18].

48   The box counting method based fractal dimension of porous media could be improved with the

49   development of advanced and high-resolution imaging techniques (e.g., micro X-ray computerized

50   tomography (micro-CT), Focused Ion Beam Scanning Electron Microscopy (FIB-SEM)), as the 3D

51   high resolution images makes it possible to characterize rock sample with high resolution [19-22].

52   Over the last few decades, several different versions of algorithms based on box counting method,

53   such as box rotate method [23,24], box flex method [25] and 2 other versions documented by La

54   Pointe [26], have been proposed to calculate the fractal dimension based on porous images.

55   However, some estimated fractal dimension of 2D and 3D sample image are larger than 3 or 2,

56   respectively, which is unreasonable [27]. According to Cai *et al.* [28], this is because the influence

57   of the minimum scale/cell size. For the improvement of the algorithm, previously, researchers took

58   different approaches to eliminate boundary effect, which is a key factor to reduce the accuracy of the

59   box counting method algorithm [23-27], the most common way is to resize the initial image by

60   adding blank pixels to make the side length of image be 2^n, n is different integers according to

61   different initial image size, then the side lengths of boxes are set as 2^m, where $1 \leq m < n$, as a result, all

62   of the initial image data can be covered by small boxes, however, this method changes the original

63   data set by adding additional data. Small boxes used in this work can cover the original data set

64   perfectly without any data loss or data implement by utilizing common divisors of the length and

65   width as box sizes to avoid boundary effect. While as appeared in the literature, there is very limited

66   research about the determination of 3D volume fractal dimension based on 3D high resolution coal

67   sample images. Especially, the relation between 3D fractal dimension and 2D fractal dimension,

68   and the relation between fractal dimension and porosity have not been discussed detailly, which are

69   very important for simplifying the fractal permeability models [16-18].

70   For the study of the relation between 2D and 3D fractal dimension, the common accepted

71   practice of obtaining the volume fractal dimension in 3D is using $D_{f3}=D_{f2}+1$ [1]. This is inferred

72   from Euclidean dimension, in which, dimension of 3D object, D_3, is 3, while dimension of 2D slices

73   that make up 3D object, D_2, is 2, then $D_3 = D_2 + 1$, however, this approach has not been proved

74   effective for fractal networks. Some researchers deduced the relation mathematically as

75    $D_{f3}=3.5-S_{D_{f2}}$, where $S_{D_{f2}}$ is the self-similar parameter of D_{f2} [29,30], however it is reported to be a

76   particular self-similar model and only for three particular projections on the Cartesian coordinate

77   planes [31]. The common practice relation was found incomprehensive to describe the relation of

78   coal samples, and the mathematic practice has already been reported to be inaccurate.

79   Recently, the influence factors on different types of fractal dimension have been studied

80   extensively, some researchers utilized low temperature nitrogen gas adsorption curve and mercury

81   intrusion curve to calculate fractal dimension of coal samples and analyze the influence factors on

82   fractal dimension. For example, Yao et al. [5] found that surface fractal dimension of coal samples

83   (R_o from 1.47% to 4.21%) has positive correlation with coal rank, Yao et al. [19] reported that

84   volumetric roughness fractal dimension of coal samples (R_o from 0.79% to 4.24%) is affected by

85   composition, such as ash, moisture, carbon, Fu et $al.$ [32] reported the volumetric fractal

86   dimension of low rank coals ($R_o < 0.7\%$) has positive correlation with moisture content. Moreover,

87   the CT technique was also widely used to calculate the fractal dimension of the coal samples. For

88   example, Liu and Nie [33] utilized box counting method to calculate fractal dimension, and paid

89   attention to influenced volatile matter content particularly, and found fractal dimension has a

90   U-shaped curve relationship with V_{daf}, Shi et al. [34] found that the 2D fractal dimension of coal (R_o

91   from 0.59% to 2.25%) has positive correlation with coal rank, Zhou et $al.$ [35] used Sierpinski-like

92   model to calculate the fractal dimension and the results showed that fractal dimension increases as

93   the pressure on the coal sample increases. In our study, the relation between fractal dimension and

94   porosity deduced theoretically and the results that calculated directly from samples were compared,

95   the results show that these results fit well with each other. Then pore area/volume fractal dimension

96   of high rank coal (R_o from 2.915% to 4.69%) was found to be mainly influenced by porosity, the

97   higher porosity, the bigger fractal dimension.

98   In this work, the box counting method was utilized to study the fractal dimension of micro-CT

99   coal images, and then the relationships among 2D fractal dimension, 3D fractal dimension and

100   porosity were discussed. In Section 2, the algorithm of the fractal dimension calculation and the

101   procedure of image processing were introduced. Then in Section 3, the computation results were

102   analyzed and verified, the relationships among 3D fractal dimension, 2D fractal dimension and

103 porosity were characterized, the influence factors were also discussed. Finally, the coal network was
104 proved self-similar and the REV (representative elementary volume) was determined, furthermore,
105 a novel method of finding the lower self-similar region size was introduced.

2. Materials and methods

2.1 Samples and coal analyses

108   The coal samples used in this study were collected from Duanshi mine, Sihe mine, Yongan
109 mine and Houcun mine in Qinshui Basin, Shanxi Province, China. The sample identification
110 numbers of them are D3-2, SH3-1, YA3-2 and H3-1, respectively. Fundamental properties, such as,
111 maximum vitrinite reflectance in oil (R_o), maceral composition and proximate analysis were
112 measured under the China National Standard GB/T 6948-2008 and GB/T 8899-2013; and the results
113 are shown in Table 1. As shown in this table, the R_o of these samples are 2.92%, 3.05%, 4.69% and
114 4.06% respectively, which indicates they are anthracite in general.

115   **Table 1** itrinite reflectance, maceral composition and proximate analysis of the coal samples.

Sample NO.	R_o (%)	Coal maceral composition (vol. %)			Proximate analysis (%)		
		Vitrinite	Inertinite	Exinite	M_{ad}	A_d	C_{daf}
D3-2	2.92	66.10	0.20	0.00	0.93	34.02	84.55
SH3-1	3.05	90.70	1.80	0.00	1.18	18.68	89.82
YA3-2	4.69	76.20	19.00	0.00	0.76	12.22	81.01
H3-1	4.06	63.80	31.70	0.00	1.03	9.33	83.35

116

2.2 X-ray CT scanning

118   The computed tomography (CT) is a non-destructive technique that can provide quantitative
119 detection of interior 3D structure of rocks, thus it has been used extensively for porous media
120 research [36]. In this study, the sample was analyzed using the GE Phoenix X-ray Nanotom
121 industrial CT instrument. The system consists of X-ray source system, detector system,
122 mechanical turntable system, image processing system. The measured samples were cylindrical

123   with a diameter of 2 mm and a height of 5 mm. The four samples were scanned with a resolution

124   of 1.1μm.

125   **2.3 Image processing**

126   The rock images obtained from micro-CT scanning, need to be processed with two main

127   steps, first reduce the noise and then do binarization before they could be used as input data to

128   calculate their properties.

129   *2.3.1 Denoise*

130   The raw micro-CT coal images normally contain noises due to the limitation of CT scanning

131   equipment itself. The noises may gloss some essential feature in the image that could significantly

132   affect the accuracy of the subsequent data analyses, and thus noise reduction is prerequisites

133   before any further implementation. In this work, the Java-based open source image processing

134   software, ImageJ, was applied to reduce the noise of the images, the median filter method was

135   utilized, and the radius was set as 2 pixels. Fig.1 shows the procedure of reducing the noise for a

136   slice of coal image. Fig.1(a) presents the slide of initial image, a highlighted yellow square area

137   was selected to be shown as an example of denoising. The selected yellow area was displayed in

138   Fig.1(b), and then it was segmented, where red denotes for the pores and fractures in the coal

139   sample, as shown in this figure, amount of isolated noises were observed. Fig.1(c) shows the

140   results after noise reduction, much less noises (mainly isolated points) were found compared with

141   that in Fig.1(b).

(a)

(b)	(c)
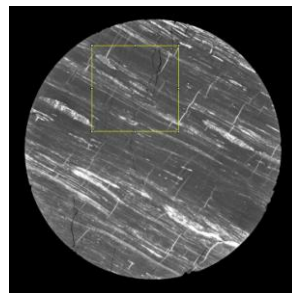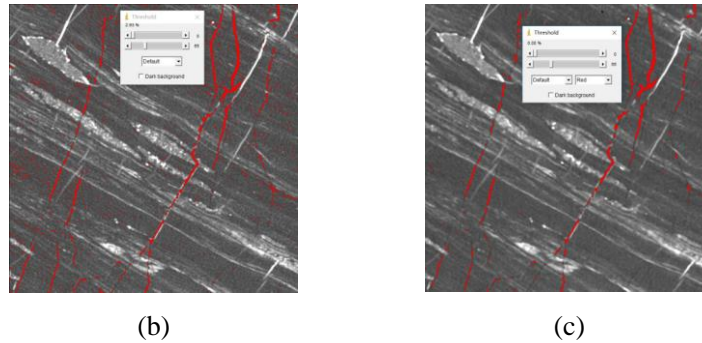
142 *Figure 1. The procedure of reducing the noise in a slice of coal sample image. (a) A slice of coal*
143 *image; (b) a selected area of the original image before noise reduction, (c) a selected area of*
144 *image after noise reduction.*

145 *2.3.2 Binarization*

146 After the coal images treated with denoise, the gray images were segmented, this was

147 accomplished by setting a threshold value first, and then the grayscale of the pixels which were

148 bigger than the threshold were set as 255 or set up as 0 if the grayscale of the pixels were smaller

149 than the threshold. This process is termed as binarization, which is essential before pore and/or

150 fracture extraction from rock images [37,38].

151 Several methods have been used to determine the threshold for binarization, such as the

152 bimodal method, porosity restriction method and the Digital Terrain Model (DTM). The grayscale

153 histogram of the conventional reservoir rock, for example sandstone, images normally contain two

154 peaks, one relates to the pores and the other relate to the rock skeleton, and thus the bimodal

155 method is widely used for determining the threshold in conventional reservoir rock images [39,40].

156 While unlike the situation of conventional reservoir rock, the grayscale histogram of coal usually

157 contains one peak, so the bimodal method is not suitable for coal image threshold estimation.

158 Currently, the porosity is normally used as criteria to determine the threshold for coal images [41],

159 and this is normally completed through an iterative process to select the threshold for matching the

160 pre-measured core scale porosity, while this approach could be problematic when there is

161 uncertainty of the pre-measured porosity, for example the coal sample may be deformed during

162 measurement under high pressure [42].

163   In this work, the DTM method, widely applied in mapping field [43], was used to determine

164   the threshold of coal images. This method was initially adopted by Taud, *et al*. [44] to estimate the

165   threshold of the micro-CT rock image for porosity calculation. And recently, the DTM method

166   was used successfully for determining the threshold value of coal sample [41]. The algorithm of

167   DTM threshold segmentation method has been described in detail previously [44]. For any CT

168   image, the relationship estimated porosity $\phi(x)$ to its corresponding gray value x can be obtained

169   [41]. The essence of calculating surface porosity of an image is to find the minimum of the

170   function $\phi(x)$, then the threshold is said to be the grey value corresponds to the minimum of the

171   function $\phi(x)$ [44]. For example, choose 4 images equidistantly from all the images of D3-2 and

172   calculate their threshold values, the results are 40, 42, 40, 43, the average is 41, so the threshold

173   value of D3-2 in this work is set as 41. Subsequently, the same method was used to determine the

174   threshold of another 3 samples.
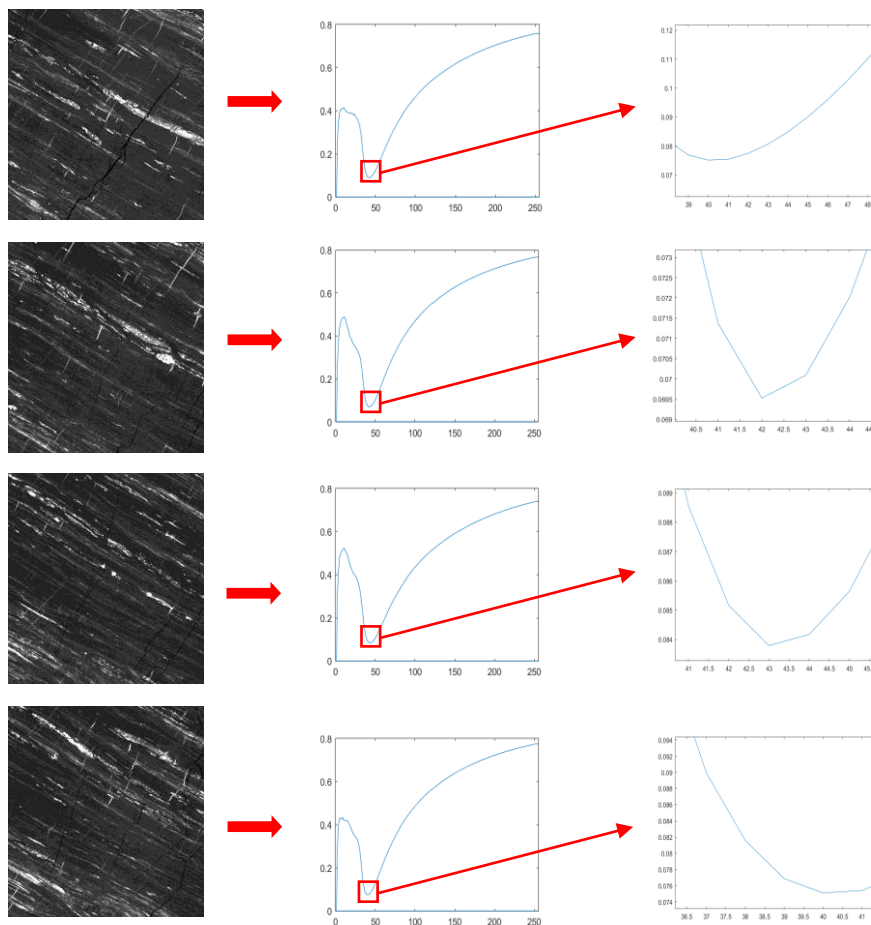
Figure 2. Porosity curves obtained by DTM threshold segmentation method, the first column is

images that are used to analyze, the second column images are the results, while the third column images are the enlarged results of the maximum value of the minimum on the curve of the second column images. x-coordinate is the gray value and the y-coordinate is porosity.

175   **2.4 Fractal dimension calculation based on coal images**

176   *2.4.1 Box counting method (BCM)*

177   The box-counting method is the one of the most well accepted method to determine the

178   fractal dimension and it has been used extensively for determining pore surface/area in 2D rock

179   images [14,15]. It contains three main steps: a. divide the binary image by boxes under different

180   length *r*, b. compute the number N of the boxes whose number of pore pixels is bigger than 1, c.

181   plot $\log N$ vs $\log(\frac{1}{r})$ on and use the linear correlation to match the data, the slop of the correlated

182   line denotes the fractal dimension. A flow chart is given in Fig.3 below to demonstrate the

183   procedures of estimate fractal dimension in 2D rock images.

```
                    ┌──────────────────────────┐
                    │   Read denoised images   │
                    └──────────────────────────┘
                                 │
                                 ▼
                    ┌──────────────────────────┐
                    │      Binarization        │
                    └──────────────────────────┘
                                 │
                                 ▼
                    ┌──────────────────────────┐
                    │         Set r            │
                    └──────────────────────────┘
                                 │
                                 ▼
    NO         ┌──────────────────────────┐        ┌──────────────┐
◄──────────────│  r satisfies requirements?│◄───────│   Update r   │
  │            └──────────────────────────┘        └──────────────┘
  │                         │ YES                          ▲
  ▼                         ▼                              │
┌────────────────┐   ┌──────────────────────────┐   ┌──────────────┐
│Plot lgN vs     │   │ Divide the image by boxes │──►│   Count N    │
│lg(1/r) and     │   │   with side length of r   │   └──────────────┘
│determine the   │   └──────────────────────────┘
│slope           │
└────────────────┘
```
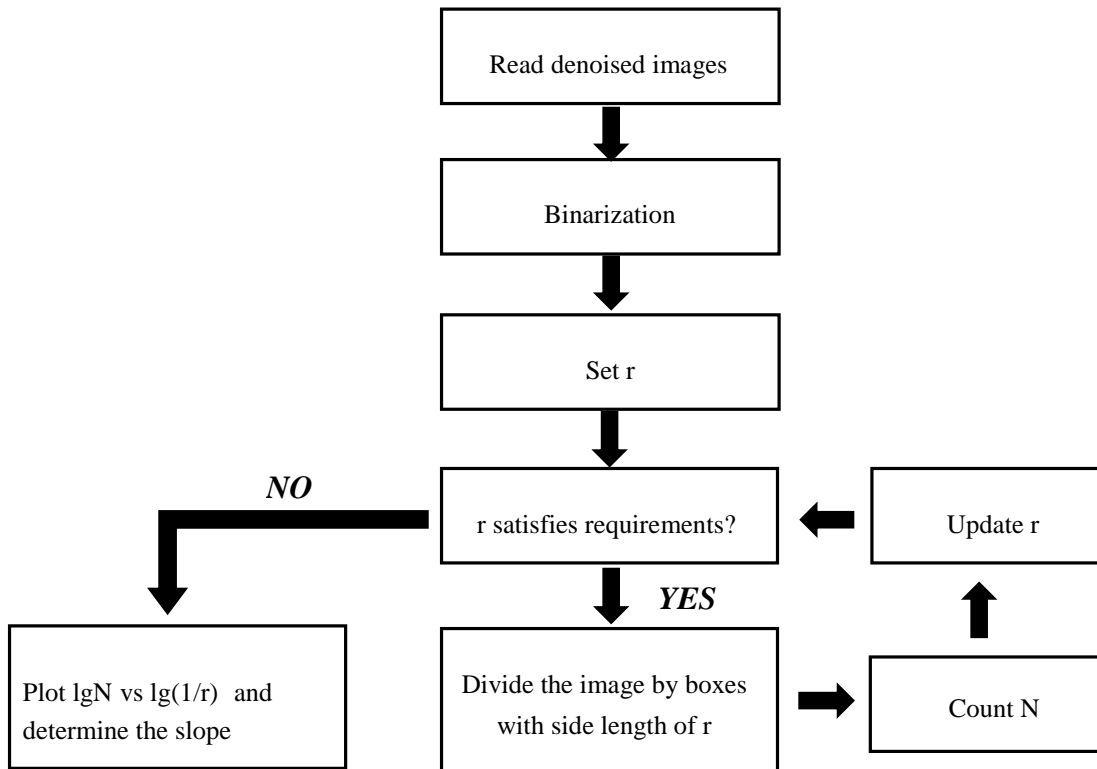
Figure 3. The flow chart of estimating fractal dimension from rock images.

184   Assuming the binary CT images with the size of M×M pixels and the gray value of 0 indicate

185   pores, which is also said to be black pixels. The square boxes (or cubes for 3D) with side length of

186   r will be used to cover the binary images, r is chosen from divisors of the length and width of the

187   image, then the original image will be divided into M/r $\times$ M/r (or M/r $\times$ M/r $\times$ M/r for 3D)

188   boxes. After that, counting the amounts of black pixels in each box, then calculate N(r), which is

189   the number of the boxes (or cubes for 3D) whose number of pore pixels is bigger than 1, a set of

190   (N(r), r) can be obtained by changing r, the data pair (-lgr, lgN(r)) can be fitted and the slop is the

191   fractal dimension according to the fractal dimension law.

192   *2.4.2 Validation*

193   According to the definition of fractal dimension, the Hausdorff-Besicovitch dimension of

194   Sierpinski Carpet (see Fig.4(a)) and Menger Sponge (see Fig.4(c)) are $D = \frac{\log 8}{\log 3} \approx 1.8928$ and

195    $D = \frac{\log 20}{\log 3} \approx 2.7268$, respectively. As shown in Fig.4(b) and Fig.4(d), excellent linear correlation

196   could be found between $\log N$ vs $\log(\frac{1}{r})$, and the calculated fractal dimension for Sierpinski

197   Carpet and Menger Sponge are 1.8928 and 2.7268, respectively, there are no deviations for when

198   compared with the analytical result, which means our program is theoretically right.

(a)   (b)

(c)   (d)
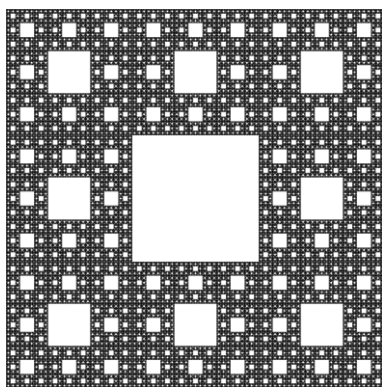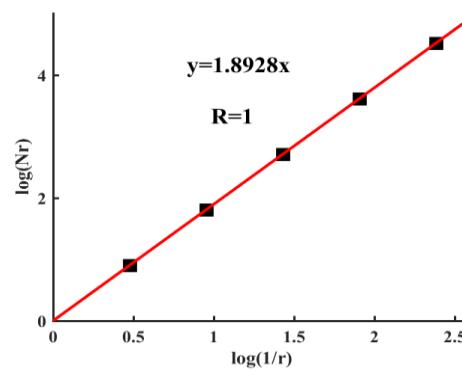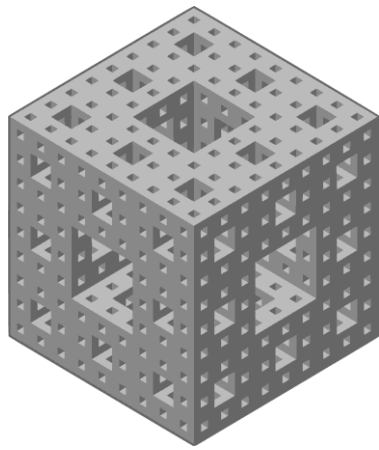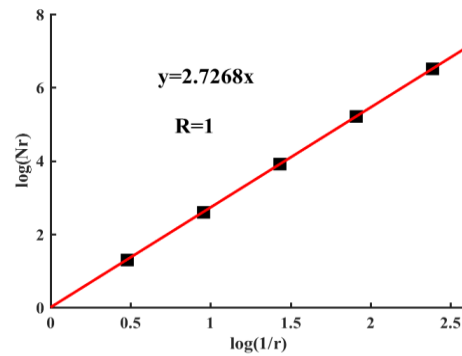
Figure 4. The fractal dimension of Sierpinski Carpet and Menger Sponge. (a) and (c) are the

images of Sierpinski carpet and Menger Sponge, respectively; (b) and (d) are fractal dimensions

of Sierpinski carpet and Menger Sponge estimated from boxing account method, respectively.

2.4.3 Computation of fractal dimension in 2D and 3D coal images

The BCM, as introduced in section 2.4.1, is used to calculate the fractal dimension directly from the rock images. The size of the 3D analyzed images are 900^3, 800^3, 400^3 and 400^3 voxels for coal sample D3-2, SH3-1, H3-1 and YA3-2, respectively. To obtain more essential data, the computation domain of 3D images constructed by different cubes initialized from 9 positions (see Fig.5).

Fig.5 gives an example of the approach that is used to generate 3D cubes with different sizes from position B. There are 9 positions, includes eight corner points, A, B, C, D, F, H, I, and the center point, E. As shown in Fig.5, 3 cubes initialized from point B are presented with different color. In this work, we increase the size of the cube with 10 pixels at each coordinate. For sample, D3-2 (with size of 900^3 voxels), it will generate 90 different cubes with size change from 10^3 to 900^3 voxels at each initial position, and thus 810 3D cubes could be constructed that initialized from the 9 points, while 9 among the 810 constructed 3D cubes are identical as the full cube with 900^3 voxels in each direction, so eventually 802 different 3D cubes could be established. With the same procedure, 632, 352 and 352 3D cubes could be constructed for SH3-1, H3-1 and YA3-2,

217   respectively. For each of the 3D constructed image, the 3D fractal dimension was calculated using

218   the 3D box counting method, and the relevant 2D fractal dimensions were presented by the

219   averaged 2D fractal dimension estimated from the slices of the 3D image.
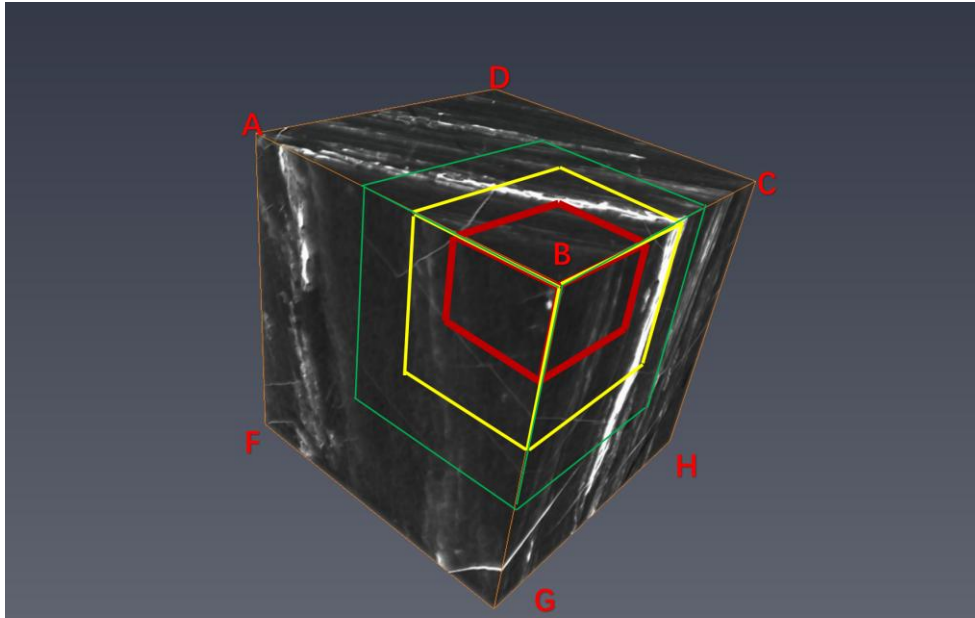
220

221   *Figure 5. An example of constructing 3D coal image with different size and initial position.*
222   *The 9 initial position contains 8 corner points, A, B, C, D, F, G, H, I, and the center position, E.*
223   *An example of 3 different 3D images that initialized from position B are highlighted with different*
224   *color.*

3. Results and discussion

225

3.1 REV of coal images

226

227   With the box counting method, the averaged D_{f3} of these 4 samples are presented in Fig.6,

228   which shows the averaged D_{f3} of 9 positions as a function of the cubic side length. As shown in

229   this figure, D_{f3} fluctuates at small computation domains and then remains constant if the

230   computation domain size surplus a critical value, and this critical value is referred as REV

231   determined by fractal dimension. As shown in Fig.6, side lengths of fractal dimension-based REV

232   of D3-2, YA3-2, H3-1 and SH3-1 are 290, 120, 120 and 160 pixels, respectively, fractal

233   dimensions of their REVs are 2.55, 2.48, 2.48 and 2.65, respectively. Fig.7 shows the relation

234   between average porosity and computation domain size, the average porosities of these 4 samples

235   become stable as the computation domain size larger than certain pixels.

236
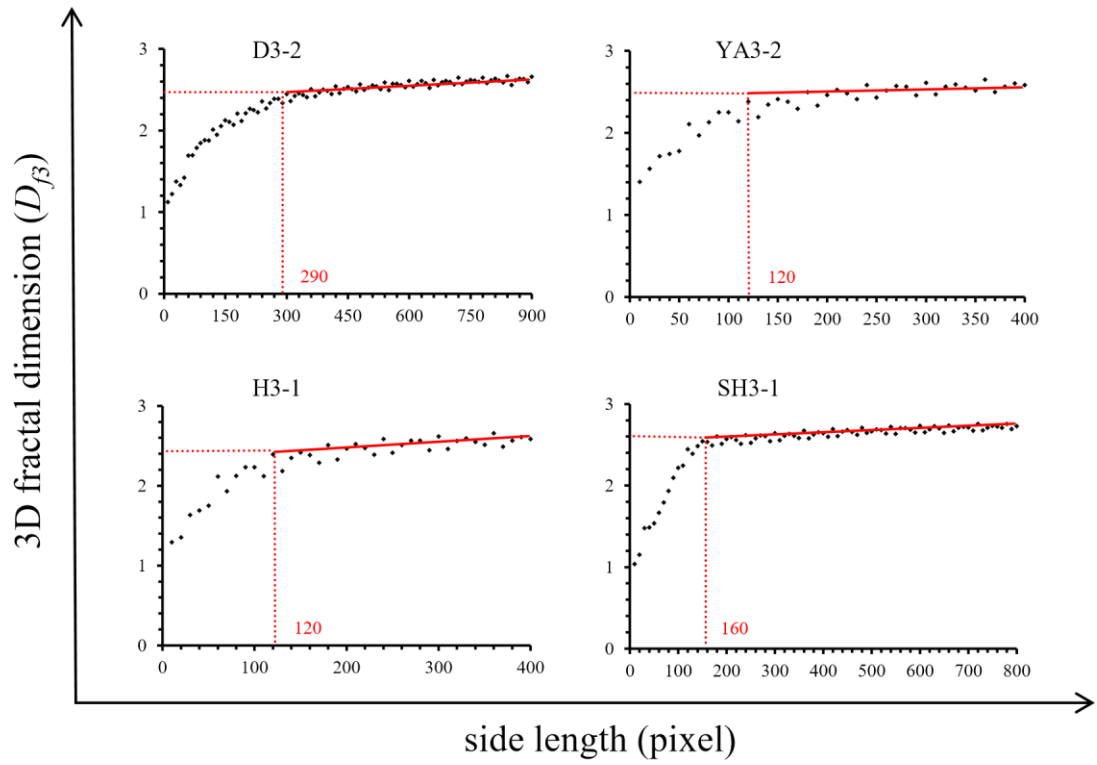
237   *Figure 6. The relation between computation domain size and average D_{f3}.*

238
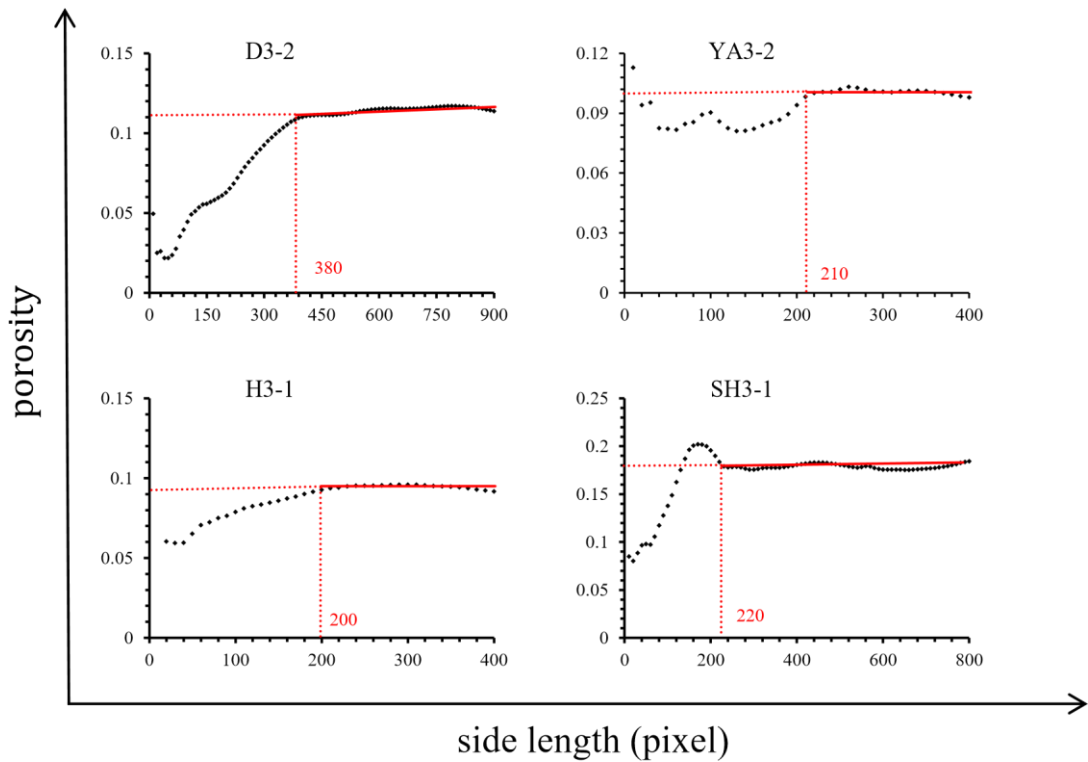
Figure 7. The relation between computation domain size and average porosity.

3.2 Relationship between D_{f3} and D_{f2}

As addressed in the literatures, the common practice of obtaining the volume fractal dimension in 3D is using $D_{f3}=D_{f2}+1$ (see Fig.8). As shown in the Fig.8, D_{f2} and D_{f3} are 2 and 3 respectively when porosity is 1, but we argue that D_{f3} calculated from 3D image whose porosity is not 100%, could be not be simply correlated with average D_{f2} by $D_{f3}=D_{f2}+1$ (see Fig.9), which presents D_{f3} as a function of D_{f2} of these four coal samples and it is clear that D_{f3} is a linear function of D_{f2}, therefore, Eq. (2) is proposed to describe the relationship between D_{f3} and average D_{f2},

$$D_{f3} = CD_{f2} + 1 \qquad (2)$$

here *C* is a parameter characterizes the relation between D_{f3} and average D_{f2}, when average D_{f2} is 2, *C* will be 1 (see Fig.8). *C* is close to 1 when average 2D fractal dimension D_{f2} larger than 1.45 (see Fig.9(a)), which means the relation between D_{f3} and average D_{f2} of high rank coal samples

252 can be expressed as $D_{f3}=D_{f2}+1$, however, there will be deviation to characterize the relation using

253 $D_{f3}=D_{f2}+1$ when average 2D fractal dimension is smaller than 1.45 (see Fig.9(b)), then Eq. (2) is

254 better than the common practice to describe this relation. Evidently, the average D_{f2} of these 4 coal

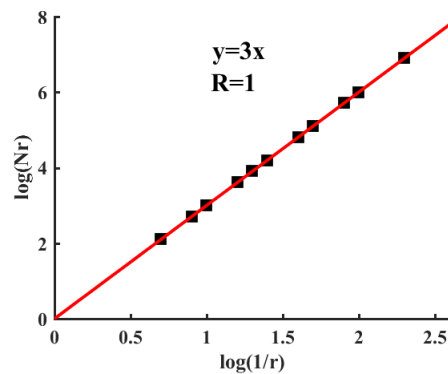255 samples from 3 different directions are very close (see Table 2).
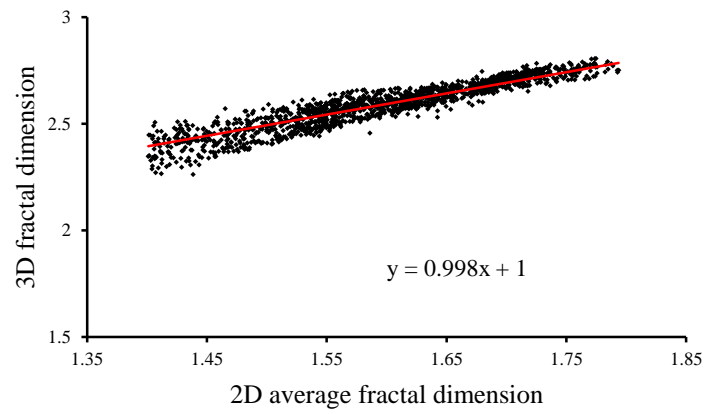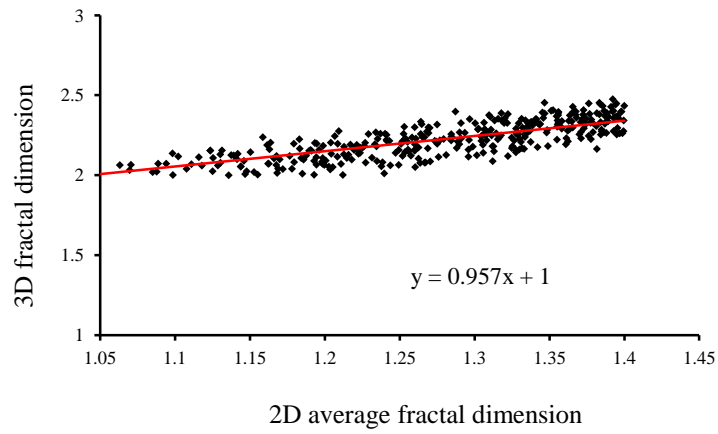

(a)
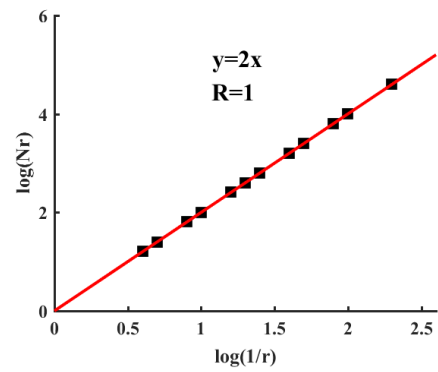
(b)
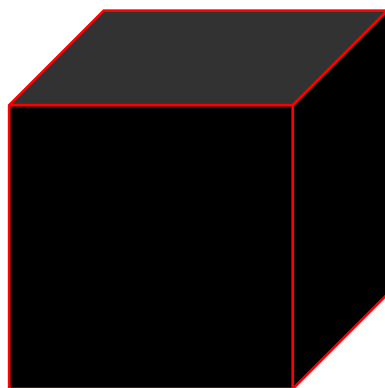
(c)

(d)

256 *Figure 8. The fractal dimensions of 2D and 3D objects with porosity is 1.*

(a)

(b)

257   *Figure 9. The relationship between 2D fractal dimension and 3D fractal dimension. (a) and*

258   *(b) are the results of average 2D fractal dimension bigger and smaller than 1.45, respectively.*

259   **Table 2**

260   Average 2D fractal dimensions from different directions

	X	Y	Z
SH3-1	1.72	1.72	1.70
D3-2	1.63	1.62	1.62
H3-1	1.57	1.58	1.58
YA3-2	1.56	1.58	1.57

261   **3.3 Relationship between fractal dimension and porosity**

262   Katz and Thompson [3] proposed a correlation between porosity and fractal dimension and it

263   is given as

264
$$\varphi = a(\frac{r_{min}}{r_{max}})^{3-D} \qquad (3)$$

265   where a is a constant of order one, φ is porosity, D is fractal dimension, r_{max} and r_{min} are upper

266   limit and lower limit self-similar region respectively. Yu and Li [45] modified Eq. (3) to allow for

267   more generalized computation domain and it is given as below in Eq. (4),

268
$$\varphi = a(\frac{r_{min}}{r_{max}})^{d-D} \qquad (4)$$

269   in Eq. (4), d denotes the Euclidean dimension of the computation domain, and d equals to 2 in two

270   dimensional spaces, and it equals to 3 in three dimensional spaces.

271   Take the logarithm on both sides of Eq. (4), the correlation can be rewritten as

272
$$\ln\varphi = -D\ln\left(\frac{r_{min}}{r_{max}}\right) + \ln\left(a(\frac{r_{min}}{r_{max}})^d\right) \qquad (5)$$

273   this equation could be simplified as:

274
$$\ln\varphi = eD + f \qquad (6)$$

275   where e and f are constants, and e equals to $-\ln\left(\frac{r_{min}}{r_{max}}\right)$, f equals to $\ln\left(a(\frac{r_{min}}{r_{max}})^d\right)$, respectively.

276   The 2D cross section of the four coal sample images are used as input to calculate the D_{f2} and

277   their relevant porosity. Fig.10 presents $\ln\varphi$ as function of D_{f2}, as shown in this figure there is a

278   linear correlation between $\ln\varphi$ and D_{f2}, which satisfies the theoretical derivation as given in Eq.

279   (6). Here we can calculate 2D r_{min} from e and f, and the 2D r_{min} of D3-2, YA3-2, H3-1 and

280   SH3-1are 5, 3, 4 and 2, respectively.

281 The relationship between porosity and D_{f3} for the 4 coal samples are also investigated. As

282 shown in Fig.11, $\ln\varphi$ is presented as function of D_{f3}. Like the cases in 2D images and expressed

283 theoretically, $\ln\varphi$ could be expressed as a linearly function of D_{f3}. We can calculate 3D r_{min} from

284 e and f, then the 3D r_{min} of D3-2, YA3-2, H3-1 and SH3-1are 76, 98, 181 and 30, respectively. The

285 3D lower limit size of self-similar region is bigger than 2D lower limit size of self-similar region,

286 and they are both smaller than the observed fractal dimension-based REV.

287 Here in the coal sample, the main contribution of porosity is the fracture/cleat system, and

288 thus r_{max} could be considered as the size of the image due to the natural extension of the main

289 fracture/cleat identified in the coal samples.
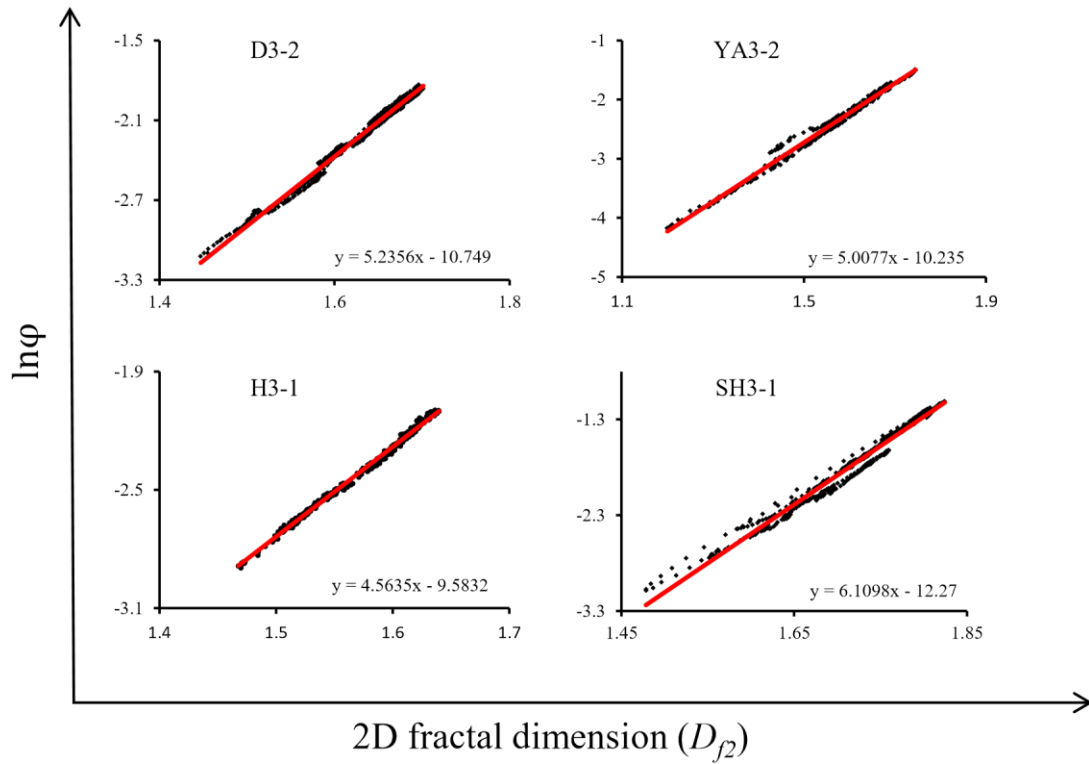
290

291 *Figure 10. The relation between D_{f2} and porosity.*

292
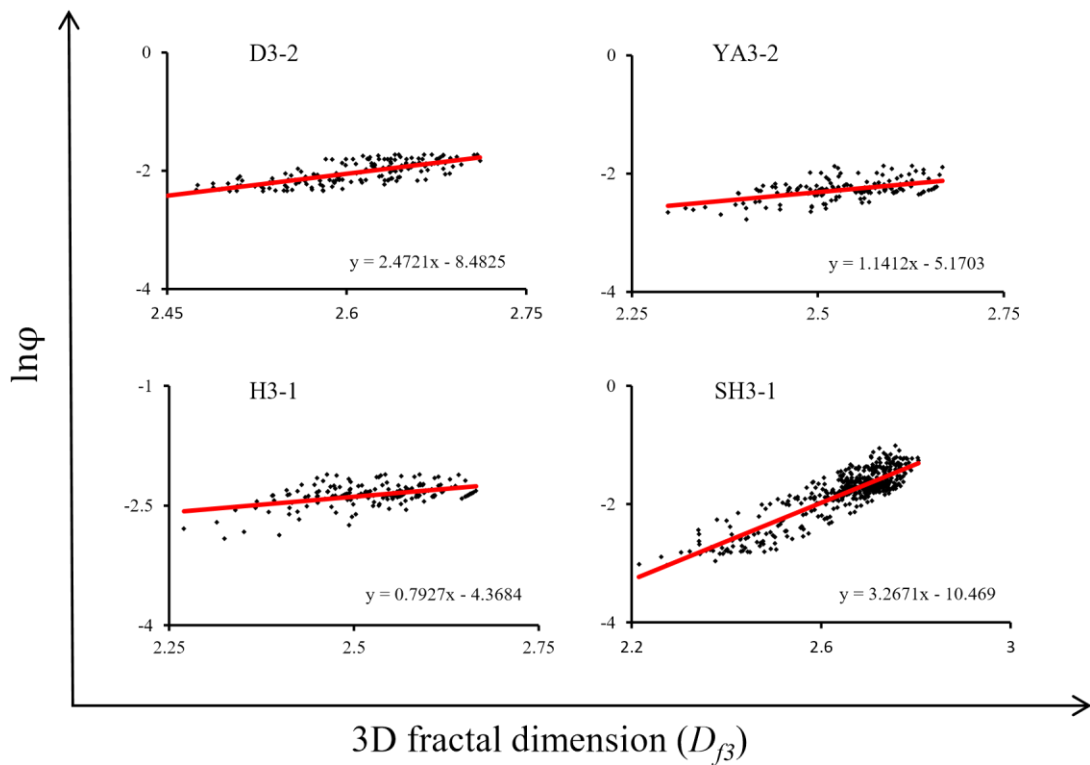
Figure 11. The relation between D_{f3} and porosity.

4. Summary and conclusion

In this work, we utilized the box counting method to estimate the fractal dimension of 3D objective, D_{f3}, and the average 2D fractal dimension, D_{f2}, directly from 3D coal samples that imaged with the advanced micro-CT imaging techniques. Based on the calculated 2D and 3D fractal dimension, the size of REV, the relationship between D_{f2} and D_{f3}, and the relationship between porosity and fractal dimension are investigated extensively. Based on our work, the detailed conclusion could be summarized as following:

- There exists the fractal dimension-based REV of 3D coal image and the bigger original image size, the bigger REV. Fractal dimensions of REVs of D3-2, YA3-2, H3-1 and SH3-1 are 2.55, 2.48, 2.48 and 2.65, respectively, which are positively correlated with porosity.

- Not like the previous result, the fractal dimension in 3D and 2D coal image could be expressed as $D_{f3} = CD_{f2} + 1$.
  - The slope of line, C, increases with the increasement of average 2D fractal dimension, D_{f2}, which is around 1 as the D_{f2} larger than 1.45 for high rank coal.
  - It was noticed that average D_{f2} of high rank coal from different directions are very close.
- Consistent with the previous theoretical derivation, we prove that porosity has an exponential relationship with fractal dimension, and it is influenced by coal composition and porosity, the lower self-similar region size can be deduced from the equation of the relation between porosity and fractal dimension.
- The minimum self-similar region, r_{min}, in 3D coal samples is larger than that in 2D sample images.

Future work of this study would be extending the proposed approach to characterize other materials, such as sandstone, carbonate, shale, and low rank coal, using the fractal theory. And look at the relationship between permeability and fractal theory. The relation between average 2D fractal dimension and 3D fractal dimension in this work was obtained based on experiments, so future work about this is to deduce the theoretical relation based on mathematic and physic theories and to improve the experimental relation.

Acknowledgments

References

329

330 [1] Mandelbrot BB. The Fractal Geometry of Nature. W.H. Freeman, New York.1983.

331 [2] Avnir D, Farin D, Pfeifer P. Molecular fractal surfaces. Nature 1984;308(15): 261–263.

332 [3] Katz AJ, Thompson AH. Fractal sandstone pores: implication for conductivity and pore

333   formation. Phys. Rev. Lett. 1985;54: 1325–1328.

334 [4] Yao YB, Liu DM, Tang DZ, Tang SH, Huang WH. Fractal characterization of adsorption-pores

335   of coals from north China: an investigation on Ch4 adsorption capacity of coals. International

336   Journal of Coal Geology 2008;73 (1): 27–42.

337 [5] Yao YB, Liu DM, Tang DZ, Tang SH, Huang WH, Liu ZH, Che Y. Fractal characterization of

338   seepage-pores of coals from China: An investigation on permeability of coals. Comput. Geosci.

339   2009;35: 1159–1166.

340 [6] Liu J, Yao YB, Liu DM, Cai YD, Cai JC. Comparison of pore fractal characteristics between

341   marine and continental shales. Fractals 2018; 26(2): 1840016-1 – 1840016-16.

342 [7] Wei W, Xia YX. Geometrical, fractal and hydraulic properties of fractured reservoirs: A

343   mini-review. Advances in Geo-Energy Research 2017; 1(1):31-38.

344 [8] Zhou SD, Liu DM, Cai YD, Yao YB. Fractal characterization of pore–fracture in low-rank coals

345   using a low-field NMR relaxation method. Fuel 2016; 181:218-226.

346   [9] Zheng SJ, Yao YB, Liu DM, Cai YD, Liu Y. Characterizations of full-scale pore size

347   distribution, porosity and permeability of coals: A novel methodology by nuclear magnetic

348   resonance and fractal analysis theory. International Journal of Coal Geology 2018;

349   196:148-158

350   [10] Zhang B, Li S. Determination of the surface fractal dimension for porous media by mercury

351   porosimetry. Ind. Eng. Chem. Res. 1995;34 :1383–1386.

352   [11] Bale HD, Schmidt PW. Small-Angle X-Ray-Scattering Investigation of Submicroscopic

353   Porosity with Fractal Properties Physical Review Letters 1984;53(6):596-599.

354   [12] Wong PZ, Howard J, Lin JS. Surface roughening and the fractal nature of rocks. Phys. Rev.

355   Lett. 1986;57(5): 637–640.

356   [13] Stallmach F, Vogt C, Kärger J, Helbig K, Jacobs F. Fractal geometry of surface areas of sand

357   grains probed by pulsed field gradient NMR. Phys. Rev. Lett. 2002;88(10-11): 105505-2 –

358   105505-4.

359   [14] Ai T, Zhang R, Zhou HW, Pei JL. Box-counting methods to directly estimate the fractal

360   dimension of a rock surface. Applied Surface Science 2014;314: 610–621.

361   [15] So G., So H., Jin G., 2017. Enhancement of the Box-Counting Algorithm for fractal dimension

362   estimation. Pattern Recognition Letters 2017;98:53-58.

363   [16] Cai JC, Hu XY, Xiao BQ, Zhou YF, Wei W. Recent developments on fractal-based approaches

364   to nanofluids and nanoparticle aggregation. International Journal of Heat and Mass Transfer

365   2017; 105:623-637.

366   [17] Cai JC, Yu BM, Zou MQ, Mei MF. Fractal analysis of invasion depth of extraneous fluids in

367   porous media. Chemical Engineering Science 2010; 65(18):5178-5186.

368   [18] Cai JC, Yu BM. A Discussion of the Effect of Tortuosity on the Capillary Imbition in Porous

369   Media. Transport in Porous Media 2011; 89(2):251-263.

370   [19] Yao YB, Liu DM, Che Y, Tang SH, Huang WH. Non-destructive characterization of coal

371   samples from China using microfocus X-ray computed tomography. International Journal of

372   Coal Geology 2009;80(2):113-123.

373   [20] Blunt MJ, Bijeljic B, Hu D, Gharbi O, Iglauer S, Mostaghimi P, Paluszny A, Pentland C.

374   Pore-scale imaging and modelling. Advances in water resources 2013;51: 197-216.

375   [21] Golab A, Ward, CR, Permana A, Lennox P, Botha P. High-resolution three-dimensional

376   imaging of coal using microfocus X-ray computed tomography, with special reference to

377   modes of mineral occurrence. International Journal of Coal Geology 2013; 113:97-108.

378   [22] Li Z, Liu D, Cai Y, Ranjith PG, Yao Y. Multi-scale quantitative characterization of 3-D

379   pore-fracture networks in bituminous and anthracite coals using FIB-SEM tomography and

380   X-ray μ-CT. Fuel 2017;209: 43–53.

381 [23] Samuel J. A method for estimating the Hausdorff dimension of a planar line pattern, M. S.

382   thesis, Colo. Sch. of Mines, Golden.1988.

383 [24] Barton CC and La Point P. Fractals in the Earth Sciences, Plenum, New York.1995.

384 [25] Pruess SA. Some Remarks on the Numerical Estimation of Fractal Dimension. Fractals in the

385   Earth Sciences. Springer US 1995;65-75.

386 [26] La Pointe L, A method to characterize fracture density and connectivity through fractal

387   geometry, Int, J. Rock Mech. Min. Sci. Geomech. Abstr. 1988;25, 421–429.

388 [27] Roy A, Perfect E, Dunne WM. Fractal characterization of fracture networks: An improved

389   box-counting technique. Journal of Geophysical Research, 2007;112: B12201-1- B12201-9.

390 [28] Cai J, Wei W, Hu X. Fractal Characterisation of Dynamic Fracture Network Extension in

391   Porous Media. Fractals, 2017;25(02): 1750023-1 – 1750023-11.

392 [29] Rachid J, Rachid H, Gerald L, Stépahnie B, Anne E. Estimation of the 3D self-similarity

393   parameter of trabecular bone from its 2D projection. Medical Image Analysis, Elsevier 2007;

394   11 (1), pp.91-98.

395 [30] Benhamou CL, Poupon S, Lespessailles E. Fractal analysis of radiographic trabecular bone

396   texture and bone mineral density: two complementary parameters related to osteoporotic

397   fractures. Journal of Bone & Mineral Research 2010;16(4):697-704.

398   [31] Akkari H, Bhouri I, Dubois P. On the Relations Between 2D and 3D Fractal Dimensions:

399   Theoretical Approach and Clinical Application in Bone Imaging. Mathematical Modelling of

400   Natural Phenomena 2008;3(6): 48-75.

401   [32] Fu HJ, Tang DZ, Xu T, Xu H, Tao S, Li S, Yin ZY, Chen BL, Zhang C, Wang LL.

402   Characteristics of pore structure and fractal dimension of low-rank coal: A case study of Lower

403   Jurassic Xishanyao coal in the southern Junggar Basin, NW China. Fuel 2017;193: 254-264.

404   [33] Liu XF, Nie BS. Fractal characteristics of coal samples utilizing image analysis and gas

405   adsorption. Fuel 2016;182: 314-322.

406   [34] Shi XH, Pan JN, Hou QL, Jin Y, Wang ZZ, Niu QH. Micrometer-scale fractures in coal related

407   to coal rank based on micro-CT scanning and fractal theory. Fuel 2018;212: 162-172.

408   [35] Zhou H, Zhong J, Ren W, Wang X, Yi H. Characterization of pore-fracture networks and their

409   evolution at various measurement scales in coal samples using X-ray μCT and a fractal method.

410   International Journal of Coal Geology 2018;189: 35-49.

411   [36] Wildenschild D, Sheppard AP. X-ray imaging and analysis techniques for quantifying

412   pore-scale structure and processes in subsurface porous medium systems. Advances in water

413   resources 2013;51: 217-246.

414   [37] Pikaz A, Averbuch A. Digital image thresholding based on topological stable-state. Pattern

415   Recognition 1996;29(5): 829-843.

416   [38] Corneloup G, Moysan J, Maynin, IE. Bscan image segmentation by thresholding using

417   cooccurrence matrix analysis. Pattern Recognition 1996;29(2): 281-296.

418   [39] Sahoo PK, Soltani S, Wong AKC. A survey of thresholding techniques. Comp. Vis. Graphic.

419   and Image Process 1988;41: 233–260.

420   [40] Moreira AC, Appoloni CR, Mantovani IF, Fernandes JS, Marques LC, Nagata R, Fernandes

421   CP. Effects of manual threshold setting on image analysis results of a sandstone sample

422   structural characterization by X-ray microtomography. Applied Radiation and Isotopes

423   2012;70: 937-941.

424   [41] Wang G, Yang XX, Chu XY, Shen JN, Jiang CH. Microscale Numerical Simulation of

425   Non-Darcy Flow of Coalbed Methane. Arab. J. Sci. Eng. 2018;43: 2547–2561.

426   [42] Yao YB, Liu DM. Comparison of low-field NMR and mercury intrusion porosimetry in

427   characterizing pore size distributions of coals. Fuel 2012;95: 152-158.

428   [43] Li Q, Ma H. The study of point-cloud production method based on waveform laser scanner data.

429   Acta Geodaetica Et Cartographica Sinica 2008;37(3): 349–354.

430   [44] Taud H, Martinez-Angels R, Parrot JF, Hernandez-Escobedo L. Porosity estimation method by

431   X-ray computed tomography. Journal of Petroleum Science and Engineering

432   2005;47(3):209–217.

433   [45] Yu BM, Li J. Some fractal characters of porous media. Fractals 2001;9: 365-372.